Fracture network characterization using 1D and 2D data of the Mórágy Granite body, southern Hungary

Tivadar M. Tóth

PII: S0191-8141(18)30284-0

DOI: 10.1016/j.jsg.2018.05.029

Reference: SG 3670

To appear in: *Journal of Structural Geology*

Received Date: 18 December 2017

Revised Date: 23 May 2018

Accepted Date: 29 May 2018

FRACTURE NETWORK CHARACTERIZATION USING 1D AND 2D DATA OF THE MÓRÁGY GRANITE BODY, SOUTHERN HUNGARY

M. Tóth, Tivadar
University of Szeged, Department of Mineralogy, Geochemistry and Petrology, mtoth@geo.u-szeged.hu

ABSTRACT

A disposal system for low- and medium-level nuclear waste in Hungary is being constructed inside the fractured rock body of the Lower Carboniferous Mórágy Granite. Previous studies proved that the granitoid massif is rather heterogeneous in terms of lithological composition, brittle structure and hydrodynamic behaviour. A significant part of the body consists of monzogranite, while other portions are more mafic in composition and are monzonites. As a result of at least three significant brittle deformation events, the area is at present crosscut by wide shear zones that separate intensively fractured zones and poorly deformed domains among them. Due to late mineralization processes, some of these fractured zones are totally sealed and cannot conduct fluids, while others are excellent migration pathways. The spatial distribution of these two types nevertheless does not show any systematics. Hydrodynamic behaviour clearly reflects this heterogeneous picture; in some places, hydraulic jumps as great as 25 m at compartment boundaries can be detected.

In this study, the fracture network of the Mórágy Granite body is evaluated from a geometric aspect using datasets measured at a wide range of scales. 2D digitized images of a hand specimen, one large (20 × 60 m) and 12 smaller subvertical wall rocks (outcrops) and 120 images from tunnel faces representing the ground level of the underground repository site were analysed. Moreover, 1D data from 13 wells that all penetrate the granitoid massif were studied. Based on measured geometric data (spatial position, length, orientation, and aperture) fracture networks are simulated to study connectivity relations and for computing the fractured porosity and permeability at different scales. The results prove the scale-invariant geometry of the fracture system. Geostatistical calculations indicate that measurable fracture geometry parameters behave as regionalized variables and so can be extended spatially. Estimated localities of connected subsystems fit very well with fault zones mapped

previously. Moreover, the spatial position of regimes of different hydrodynamic behaviours can be explained by connectivity relations both regionally and within wells.

INTRODUCTION

A disposal system for Hungary's low- and medium-level nuclear waste is being constructed inside the fractured rock body of the Lower Carboniferous Mórágy Granite. There are only a few outcrops available for studying the rock on the surface; the granite body is essentially covered by younger Pliocene and Pleistocene sediments. As rock heterogeneity relations as well as large-scale structures of the area can hardly be examined by traditional outcrop survey or using remote-sensing approaches, numerous wells penetrating the granite body reveal the petrological and structural circumstances. Moreover, two access tunnels were excavated underground.

Fracture systems play an essential role in fluid flow and transport processes in hard rock bodies. Over the last few decades (e.g., Maros et al., 2004, 2010), a detailed structural geological evaluation of the faults and fault systems in the Mórágy Granite has been completed; the most important deformation zones are well-known and have been published on high-resolution maps. Nevertheless, fracture networks at micro- and meso-scales, which play a significant role in hydrodynamic behaviour of the hard rock body (Anders et al., 2014), are basically unknown and are studied in the framework of the present project. The most essential questions are whether the single fractures form a communicating network or not, how large the communicating subsystems are and where they are located. To answer these questions, fracture networks are simulated based on measurable geometric parameters. Fracture networks are usually handled as scale invariant geometrical objects (e.g., Korvin, 1992, Turcotte, 1992, Long, 1996, Weiss, 2001). To test whether the fracture network of the Mórágy Granite can be examined by the corresponding methodology, fracture systems at a wide spectrum of scales (surface outcrop, tunnel faces, borehole and hand specimen data) are evaluated simultaneously using the same set of methods. That is, data used for simulation work are received by a combined analysis of 1D and 2D fracture patterns. Modelling requires geometric data regarding fracture size distribution, spatial density and orientation. Simulated models are afterwards available to understand features of the fractured rock body concerning hydrodynamic behaviour, such as connectivity, porosity and permeability.

GEOLOGICAL BACKGROUND

The Bátaapáti Site is located in the southern part of Hungary (fig. 1); the Carboniferous Mórágy Granite Formation (MGF) was selected as the repository of low- and intermediate-level radioactive wastes. Petrographically the MGF was described by Király and Koroknai (2004) as a porphyritic monzogranite intercalated with a more mafic variety of monzonitic composition without a sharp contact (fig. 2). According to the recent models the combination of the two granitoid rock types developed through a magma-mixing process. The whole rock body is also crosscut by swarms of aplitic dykes of various widths. Two major deformation events developed the ductile structure of the MGF (Király, Koroknai, 2004). The magma-mixing process coincided with formation of a generally NE-SW striking igneous foliation mostly with a steep NW dip. During the next phase, deformation resulted in steeply foliated mylonitic zones, basically with a NE-SW strike again. The upper several tens of metres of the granitoid body are strongly altered and weathered and are covered by Miocene, Pliocene and Quaternary sediments with a thickness of approximately 50 m on the hilltops and thinning towards the valleys. As a consequence, only a few surface outcrops exist that are available for petrological and structural study. Many details of mineralogical, geochemical and petrological circumstances of the MGF, not directly concerning the present project, are presented in Király (2010) and references therein.

The brittle deformation history of the area and the mechanisms of different structural events are discussed in detail by Maros et al. (2004). Most structures exhibit two typical orientations: NE-SW (the dominant set) and perpendicular to this (NW-SE) (fig. 1). Small-scale fracture orientations are very similar to those appearing at large-scale zones (Benedek and Molnár, 2013). When studying fracture networks from a geometric aspect, fracture size appears to be related to the distance from major fault zones; larger fractures appear to cluster preferentially around them (Benedek and Molnár, 2013). Nevertheless, length exponents were found varying within a very narrow range (2.15–2.44) at different scales (outcrop scale: 0.4–7 m trace length, vertical seismic profile measurements: 6–40 m trace length, seismic line measurements: 100–400 m trace length, Benedek and Dankó, 2009).

Generally, a fractured reservoir system can be divided into two subsystems; more permeable discontinuities surround a less permeable matrix (Neuman, 2005). This theoretical model is the basis of the hydrostructural concept of the MGF as well (Molnár et al., 2010). Benedek and Molnár (2013) distinguish two hydraulic domains inside the fractured granitoid body; less transmissive blocks and more transmissive zones (LTBs and MTZs, respectively). Nevertheless, the definition of the boundaries between these two domains is highly subjective.

The MTZs follow both NE-SW and NW-SE directions, with the most significant flows observed along the NE-SW zones. Fractures inside an LTB, on the other hand, cannot be represented by any single characteristic orientation. Although hydraulically active fracture zones are frequent in the study area, fracture clusters are not entirely interconnected. As a consequence, there is no hydraulic connectivity between all points of the studied region (Benedek and Dankó, 2009). According to Benedek et al. (2009) such a compartmentalization is not exclusively the result of fracture geometry, but in part the consequence of intensive secondary mineralization of certain fracture zones. At a site scale, the resulting strongly compartmentalized character of the fracture system causes the high complexity of the flow pattern as well. Neighbouring compartments usually have slightly different heads (1–5 m), while hydraulic jumps at compartment boundaries defined by sealed faults may be as great as 5–25 m. In general, hydrodynamic behaviour and especially the calculated transmissivity is significantly different for the two differently deformed regions, varying being 10^{-12} and 10^{-6} m^2/s for the fresh granite of the LTBs and $8*10^{-6}$ and $2*10^{-5}$ m^2/s for the MTZs (Balla et al. 2004, Rotár-Szalkai et al, 2006).

SAMPLES

In this study of the brittle structures of the Mórágy granite body, 1D and 2D information collected from diverse localities and scales were evaluated. The most detailed 2D fracture network dataset is represented by a subvertical outcrop, 20 × 60 m in size, at the SW part of the study area. From the same outcrop, a hand specimen (20 × 30 cm in size) was investigated as well. In addition to the hand specimen and the whole wall, 12 smaller, equally sized rectangular portions of the wall have been documented and evaluated.

Additional 2D fracture network data were derived from tunnel faces representing the ground level of the underground repository site (fig. 1, inset). Altogether 120 JointMetriX3D (Gaich et al., 2005, Deák and Molnos, 2007) images were handled with an equal 20 m lag between the neighbouring sampling points. At least 300 single fractures were digitized and evaluated in each JointMetriX3D image.

The series of intersection points between the fracture system in the real 3D and a line (usually a borehole) defines a 1D data set. 1D fracture data were obtained by evaluating well-logs (BHTV, acoustic borehole televiewer; Zilahi-Sebess et al. 2003) and core scanner (CS, Maros and Palotás, 2000) images from 14 wells, representing the whole study area (fig. 2).

METHODS

Fracture networks can be characterized from numerous structural geological points of view and by diverse measurable geometric parameters. In the latter approach, each single fracture must be represented by an appropriate geometric shape. In most approximations a polygon or a circle is used for this reason (Neuman, 2005). Hereafter, this last approach is followed, and so the most important geometric parameters to define a fracture are length (diameter), spatial position of the centre and orientation. To calculate porosity and permeability data for the fracture network, the fractures must have positive volume, so instead of pure circles, each fracture is represented by a flat cylinder geometrically (parallel plate model, Witherspoon et al., 1980; Neuzil, Tracy, 1981; Zimmerman, Bodvarsson, 1996). Furthermore, in order to understand spatial behaviour of fracture networks, a large set of discrete fractures should be studied simultaneously, and distributions of length, aperture, orientation (strike and dip) and spatial density of fracture midpoints are used. Abbreviations of the geometric parameters applied are summarized in Table 1.

During the fracture network modelling process three sets of methods are used. 1) The first of them deals with determination of fracture network geometric parameters. 2) Prior to fracture network simulation using the above parameters, they should be interpolated for the studied area. 3) Finally, appropriate simulation software should be applied for 3D fracture network modelling.

Geometric parameters of fractures

Length distribution

Both concerning conductivity and fluid storage, length distribution is an essential parameter of fracture networks. According to numerous previous studies, fracture lengths follow a power law distribution (Yielding et al., 1992, Min et al., 2004), that is $N(L) = F * L^{-E}$. Using an appropriate number of single fractures (at least 300), on any 2D surface, the two parameters E (the length exponent) and F can be determined by image-analysis methods on digital photos (Healy et al., 2017). First, the frequency distribution function of fracture trace lengths measured on any photo were plotted. When computing the histogram, the number of classes (k) was determined so that $k = 2 * \mathrm{INT}(\log_2(\mathrm{N}(L))$. Length exponent is afterwards the slope of the best fit line on the Log(L)-log(N(L)) plot. Because of representativity defects, the smallest and longest fractures usually do not fit to this line and so must be left out of the analysis. This approach was followed when evaluating data of the outcrop, the hand specimen and the tunnel faces (fig. 3). Instead of using the histogram on doubly logarithmic axes, to find the best fit line Rizzo et al. (2017) suggest to apply maximum likelihood estimator.

To determine the length exponent in the case of 1D data sets, the same equation ($N(L) = F * L^{-E}$) can be utilized as previously presented. The mathematical background of how to obtain the E parameter using 1D point series is too long to recall here; it is described in detail in M. Tóth (2010). Using this approach, a unique E parameter has been determined for each studied well (fig. 2).

Spatial density of fracture midpoints

Numerous previous studies proved that fracture systems behave geometrically in a fractal-like pattern (Barton and Larsen, 1985, La Pointe, 1988, Hirata, 1989, Matsumoto et al., 1992, Kranz, 1994, Tsuchiya and Nakatsuka, 1995, Roberts et al., 1998, among others). Consequently, the spatial distribution of single fractures can be characterized by the fractal dimension of the fracture midpoints. Fractal dimension is computed using the box-counting method, applied to fracture network analysis by numerous authors previously (Mandelbrot, 1983, Mandelbrot, 1985, Barton and Larsen, 1985, Barton, 1995). Here, a non-overlapping regular grid of square boxes was used during the box-counting analysis. In the algorithm, the number of boxes (N(r)) required to cover the pattern of fracture seeds is counted. Fractal dimension is calculated by computing how this number changes in making the grid finer, afterwards: $N(r) \sim r^{-D}$ (fig. 3). For box-counting calculations, the BENOIT 1.0 software was used Benoit 1.0 (Trusoft, 1997).

To determine fractal dimension in the case of 1D scanlines, a fractional Brownian motion analysis was followed as described in detail in M. Tóth (2010). As R/S (Rescaled Range) analysis applied in determining fractal dimension along a scanline needs at least 400 points (single fractures) to reach reasonably low uncertainty (Katsev and L'Heureux, 2003), D parameters were calculated every 25 m as a minimum. Within this depth interval each well crosscuts the desired number of fractures, making D logging along the wells possible.

Fracture aperture

Most previous studies (de Dreuzy et al., 2002, Ortega et al., 2006) confirm that, similar to length, aperture data follow a power law distribution. Nevertheless, the two parameters are not independent of each other; instead, a tight linear relationship is also suggested between them such that: $a = A * L + B$ (Pollard and Segall, 1987, Gudmundsson et al., 2001). Both measurements on naturally fractured rock bodies and theoretical deliberation confirm that a/L

typically varies by an order of magnitude of 10^{-2} to 10^{-3} for most rock types (Opheim and Gudmundsson, 1989, Vermilye and Scholz, 1995). In the studied case, the aperture was measured exclusively on the hand specimen under a binocular microscope (50× magnification). For each microfracture, aperture was determined at a minimum of 3 points.

Fracture orientation

In the near-well fracture network modelling procedure, orientation data (dip direction and dip angle) of individual fractures obtained by BHTV interpretation were used (Szongoth et al., 2004). For modelling the underground site, orientation data measured in the closest well (Üh-2) were used.

Interpolation of the fracture network parameters

The *D* values were computed for each well for every 25-m interval making generation of a series of horizontal *D*-maps possible. Nevertheless, the reduced number of wells deemed reliable for mapping did not allow application of sophisticated geostatistical methods (semivariogram analysis and interpolation using kriging). Therefore, for interpolation and extrapolation, the minimal curvature method (Dietze, Schmidt, 1988 and references therein) was chosen in a grid net of 100 × 100 × 25 m sized cells. In the case of the underground repository site, georeferenced photos are available for precise calculations. To understand the spatial variability of fracture parameters, semivariogram and variogram surfaces were computed using the Variowin 2.2 software (Pannatier, 1996). Considering the variogram data, ordinary kriging was applied for parameter interpolation. During the procedure, 30 × 30 × 30 m sized cells were used.

In both studied cases (whole area and underground site), the interpolated fracture parameters served as input data for the fracture network modelling procedure.

Fracture network modelling

During a previous modelling study in a small subarea of the recent study area, Benedek and Molnár (2013) used the Poisson point process as a spatial model for fracture localization. In that model, fractures represent a random function in space. Hereafter, for simulating fracture networks in 3D, the RepSim code was used (M. Tóth, 2010, M. Tóth and Vass, 2011, Bauer and M. Tóth, 2016). In this DFN (discrete fracture network) software penny-shaped single fractures are generated in a stochastic manner with a given parameter set of (D, E, F, α, β) measured in the real fractured rock body. Thanks to the stochastic approach in the fracture system generation, numerous equally probable networks can be simulated and evaluated. Aperture is calculated for each discrete fracture in a deterministic manner assuming the aforementioned length-aperture relationship (Odling, 1993). One of the most essential features of a simulated fracture network is the size and spatial position of its communicating subsystems. In the applied software, they can be found using a properly optimized trial-and-error algorithm (M. Tóth and Vass, 2011).

Fractured porosity can be defined as

$$\Phi = \frac{Vf}{V} . \qquad (1)$$

In the case of cubic cells $V = r^3$, the total volume of the fractures inside a certain cube (V_f) can be approximated well by the lower Riemann sum, that is,

$$\mathrm{Vf} = \sum_{i=1}^{n} \sum_{j} \frac{l_{ij} \cdot a_{ij} \cdot r}{n} , \qquad (2)$$

and the porosity is in the form of

$$\Phi = \frac{1}{n * r^2} \sum_{i=1}^{n} \sum_{j} l_{ij} \cdot a_{ij} \qquad (3)$$

The permeability of a fractured rock mass can be represented by a 3×3 permeability tensor. In the RepSim code, it is calculated using the slightly modified algorithm of Oda (1985). Thus, under Darcy's law,

$$v_i = \frac{g}{\mu} \cdot \rho \cdot k_{i,j} \cdot J_i \qquad (4)$$

where v is the specific flow rate, μ is the dynamic viscosity, ρ is the density of the fluid, and ***J*** is the hydraulic gradient. On the other hand, as fluid can percolate only along fractures, over a given volume,

$$v_i = \frac{1}{V} \cdot \int v_i^f \cdot dV^f \qquad (5)$$

where v^f is the flow velocity in a discrete fracture. This is approximated ad libitum by

$$v_i = \frac{1}{V} \cdot \sum_f v_i^f \cdot V^f \qquad (6)$$

Under the cubic law, where assuming laminar flow within a fracture (parallel plate model, Witherspoon et al., 1980, Neuzil and Tracy, 1981), the specific flow rate is proportional to the square of the fracture aperture, and

$$v_i^f = \frac{1}{12} \cdot \frac{g}{\mu} \cdot \rho \cdot a^2 \cdot J_i^f\,, \qquad (7)$$

where $\mathrm{J}_i^{\,f}$ is the *i*th component of ***J*** projected onto the *f* fracture, that is, as

$$J^f = J - (n \cdot J) \cdot n \text{ and} \qquad (8)$$

$$J_i^f = \sum_j (\delta_{ij} - n_i n_j) \cdot J_j\,, \qquad (9)$$

where δ_{ij} is the Kronecker delta symbol. Thus, finally comparing *(4)* and *(6)* according to Oda (1985),

$$\mathrm{k}_{i,j} = \frac{1}{12} \cdot (\mathrm{P}_{kk} \cdot \delta_{ij} - \mathrm{P}_{ij})\,, \qquad (10)$$

and under the discretization solution of Koike and Ichikawa (2006), considering that in the case of cubic cells $V = r^3$,

$$P_{ij} = \frac{1}{r^3} \cdot \sum_f a^3 \cdot l \cdot n_i \cdot n_j\,. \qquad (11)$$

Finally, using the lower Riemann sum approximation

$$P_{ij} = \frac{1}{k \cdot r^3} \cdot \sum_k \sum_f a^3 \cdot l \cdot n_i \cdot n_j \qquad (12)$$

and

$$P_{kk} = P_{11} + P_{22} + P_{33} \ , \qquad (13)$$

where n_i and n_j are the normal vector projections of the given fracture on the particular axes.

Using the RepSim code, a fracture network model was generated along each well for a 100 × 100 m sized column surrounding the well. During modelling, orientation data measured in the given well were used together with the *E* value of the well and *D* values for each 25-m-long segment. In this way, modelling of real fracture geometry at any depth interval becomes possible for each well. Parameter interpolation between wells resulted in an *E*-map as well as a series of *D*-maps with a 25-m lag. Using these maps, a spatial fracture network model was generated for the whole studied rock volume (500 × 1000 × 400 m in size).

For modelling the underground site, the size of the whole modelled block is 300 × 300 × 150 m. Both above and below the horizontal repository site a 75 m-thick rock body was involved. As there are reliable data exclusively from the shafts themselves, input geometric data were assumed identical vertically. The aim for modelling a significant volume instead of only the horizon of the repository site itself is to let fractures combine communicating systems in 3D. For simulation, the whole modelled block was divided into 10 × 10 × 15 parts of cells. Finally, the results of 10 independent runs were evaluated and compared. In each case, fracture models were evaluated concerning size and spatial position of the communicating subsystems, and typical values for fracture porosity and elements of the permeability tensor were computed.

RESULTS AND DISCUSSION

Fracture network of the outcrop

By analysing the digital images, altogether more than 6500 single fractures were recognized and digitized on the subvertical granitoid wall (fig. 3a), while on the hand specimen, 750 single microfractures were found and digitized using pictures taken by a binocular microscope. Length data (fig. 3b) clearly infer the accepted power law distribution; on the ln(N(L)) – ln(L) plot a straight line with an E = -2.48 fits very well (fig. 3c). On the diagram a significant misfit can be observed for both the shortest and the longest fracture classes. On the one hand, it is caused by uncertainty in digitization of short (and thin) fractures; on the other hand, the studied volume is not large enough to estimate the number of the longest fractures. Evaluation of the 12 portions of the wall resulted in distribution functions of identical appearance and numerical results (E = -2.46 ± 0.02). The same value for the single hand specimen is E = -2.36 (750 single fractures). Calculations on the wall prove that fracture lengths in the studied granitoid body follow power law distribution with length exponent values that are very similar for a wide range of scales. This result is in agreement with Benedek and Dankó (2009), who did not find any fundamental difference between the trace lengths of fractures with different orientations and sizes.

Concerning spatial density, the fractal dimension of the fracture seeds calculated for the 12 portions of the wall is D = 1.56 ± 0.07 with a maximal value of D = 1.64 (fig. 3d, e). The same value for the whole wall is D = 1.56, while in the case of the hand specimen, a slightly smaller number was obtained; D = 1.45. Detailed microscopic measurements suggest a linear relationship between fracture length and aperture values with $a/L \sim 2.7 \cdot 10^{-2}$. D and E values determined at different scales in the case of the wall are plotted in fig. 4.

Near-well fracture networks

Using the approach detailed by M. Tóth (2010), a single E value has been computed for each well, using BHTV and CS data. The values vary in a rather wide range, between 1.09 and 2.64, suggesting significantly different length distributions in different parts of the study area. As D values, computed at every 25 m, show smooth trends along each well without any unexpected jump between neighbouring depth intervals (fig. 5), spatial continuity of fracture density is suggested. The average D values in the wells change in the range of 1.12–1.83, pointing to very differently dense networks for different wells. E and average D values for each well are plotted in fig. 4. Using an essentially different methodology, Benedek and Dankó (2009) found that fractal dimensions of the fracture networks are very close to 1.0 along boreholes, suggesting a random fracture pattern in space without any significant change. A definite advantage of the present approach compared to that used previously is the ability to sensitively follow variation in fracture geometry parameters along wells and so simulate fracture networks much more reliably.

The fracture network models generated exhibit visibly more and less fractured segments along each well (for a typical example, see fig. 6). Studying connectivity relations, these networks usually can be subdivided into communicating and not communicating intervals depending basically on the variation in *D* value along the well (fig. 6a-c). In fact, these patterns clearly infer that the fracture system of the granitoid body is far from homogeneous. Instead, there are wide zones in almost each well with a fracture system below the percolation threshold. Studying the hydrodynamic behaviour of the fractured granitoid body, Benedek and Dankó (2009) indicated the coexistence of small-scale hydraulic head-scattering and large hydraulic head jumps along individual boreholes. They also published hydraulic head profiles for a few wells, such as for Üh-22 (fig. 6d). Comparing the near-well fracture network model (fig. 6b) and especially the position of the communicating subsystem of the modelled fracture network (fig. 6c) to the head profile suggests a clear coincidence. That is, hydraulic head tends to jump at the depth horizon, where a connected fracture network could have developed. Balla et al. (2004) conclude that abrupt head jumps are basically caused by highly altered fault core zones rather than a sparse fracture network. Although this interpretation cannot be proved here, the results of all modelled wells suggest that head jumps can definitely be linked to the border of intensively and barely fractured domains. More exactly, the head tends to jump at depth intervals where a connected fractured zone and the host rock with an unconnected network meet. Nevertheless, significant head jump is typical neither in these wells, where most fractures are connected, nor in these cases, where the whole fracture system is below the percolation threshold.

Whole-area fracture model

All previous studies noted that the fracture network of the MGF is highly heterogeneous consisting of intensively and barely fractured domains. Moreover, alteration of the host granite and the fault rocks following brittle deformation events resulted in open and closed fractures without any spatial consistency. Benedek and Dankó (2009) prove that, basically because of late mineralization processes, a network of single fractures larger than ~10 m in diameter form the hydrodynamically active system in the area, while the role of minor fractures is subordinate. For this reason, when computing the communicating subsystems based on the RepSim fracture model of the whole study area, short fractures were left out of the calculation.

The map in fig. 7a shows the fracture centres of all single fractures (longer than 10 m) of the largest connected subsystem projected onto the surface. This picture suggests a rather dense network in the SE, while to the north, a much sparser but still communicating system is typical. These two major domains are separated by a wide zone in the middle with a non- or hardly communicating (in the western end of the area) set of fractures. This area coincides exactly with the zone defined as the “main sealing feature” by Benedek et al. (2009), which separates two hydrodynamic regimes. While all wells south of this zone communicate with each other hydrodynamically as do those north of it, the northern and southern regimes are unconnected. The present model suggests the opposite to the previous interpretations; the main reason for existence of the two realms is that in the middle zone the fracture network is below the percolation threshold.

Comparing the most intensely fractured zones appearing in the horizontal section of the model at 0 m a.s.l. to those mapped previously, a tight agreement becomes clear (fig. 2, 7b). Both direction (NE-SW) and locality of all these zones fit well on the two maps suggesting that even map-scale shear zones can be followed based exclusively on microfracture geometrical data. In the N-S striking vertical section (fig. 7c), a swarm of parallel fault zones can be sketched in the south, while north of the hardly fractured middle realm, a single fault zone appears in good agreement with the structural map. In agreement with the current interpretations, all these zones are steeply dipping. Nevertheless, the gently dipping character of the zone in the middle of the central area does not fit the previous models and needs further study.

In the monzogranite-dominated area (fig. 2), tight covariation between fractal dimension and the E parameter is evident, so for most wells, large E values characteristically coincide with the smallest average D values, and vice versa (fig. 4). That is, in this rock type sparse fracture networks are characterized by short fractures (small D, large E values). Moreover, as the fracture network becomes denser (increasing D), single fractures become longer (decreasing E). The two wells that do not fit this trend, Üh-27 and 28, both penetrate the granitoid massif at the border of the monzonite-dominated realm in the north (fig. 2, fig. 7b, c). Here, small D values coincide with small E values, that is, a sparse network of long fractures is typical at all scales. As the two regions of the study area with different fracture geometry values coincide well with those characterized by different lithologies, one can assume that monzonite and monzogranite have different rheological behaviours. Dependence of the geometry of scale invariant fracture networks on the structure and composition of rock type has been proven by many authors previously (e.g., Bean, 1996, Marsan and Bean, 1999).

Concerning the study area, Benedek and Molnár (2013) proved that large fractures tend to appear clustered preferentially around major shear zones. Recent results show that beyond that, microfractures crosscut by wells can be used in predicting large-scale shear zones underground.

Fracture network of the underground site

E and *D* data detected in the tunnel faces vary in a range of 1.03–2.27 and 1.50–1.86, respectively (fig. 4). Variography, fulfilled for spatial interpretation of these data around the underground site, proves that both variables (*E*, *D*) are continuous in space. Nevertheless, the two semivariograms differ significantly from each other. For the length exponent, the theoretical semivariogram shows a large nugget effect (approximately 70% of the total variance); after reaching the sill, the variogram values do not change significantly (fig. 8a). This variogram can be best approximated by a combination of a nugget effect (0.102) and a spherical model (range: 73.5 m, sill: 0.05). The low degree of spatial dependence, indicated by the large nugget effect, can also be postulated based on the variogram surface in the case of the *E* parameter (fig. 9a).

Spatial behaviour of the other key parameter (*D*) is much different (fig. 8b). Here, the nugget effect does not reach even one-third of the total variance. The best fitted theoretical variogram consists of two Gaussian models (ranges: 30 and 160 m, respectively) in addition to the nugget. Remarkable anisotropy, suggested by the directional variograms (NE-SW; NW-SE, fig. 8c, d), is also confirmed by the variogram surface, which clearly indicates the NE-SW orientation of the studied structure (fig. 9b). Although the nugget effect is much smaller than is typical for the *E* parameter, it is still rather high, calling attention to the role of measurement uncertainty or spatial sources of variation at distances less than the sampling interval or both (Clark, 2010). On the other hand, it is clear that both the spatial density and the length exponent are regionalized variables and so are able to be extended spatially.

Based on the nested structure of the variogram (*D*), in the studied case, a complex fracture network can be assumed what is a combination of two anisotropic systems with remarkably different ranges (30 and 160 m, respectively). Coexistence of these two systems clearly reflects the known structure of the Mórágy Granite, namely, the presence of less transmissive blocks surrounded by the most transmissive zones. Therefore, for interpolation of the *D* parameter at the first step, the nested semivariogram was used with NE-SW anisotropy of 1.5. Afterwards, the two structures were modelled independently. On the parameter map of the large-scale structure, a densely fractured zone becomes evident on the NW part of the area with a clear NE-SW orientation, while on the SE part a network with much smaller density appears. Interpolation using only the small-scale structure results in a much more detailed map. The final map of the *D* parameter (each cell is 30 × 30 m in size) was reliable for fracture network simulation and was computed using the nested variogram is shown in fig. 10a, b. While the presence of the NE-SW oriented zone in the NW corner is still obvious, another intensely fractured region becomes visible in the SE. Nevertheless, it is worth mentioning the appearance of a hardly fractured block in the middle of the studied underground site. Based on the map of the length exponent, larger *E* values are typical in the western part of the area (fig. 10c, d).

Using these maps, 10 independent fracture networks were simulated using the RepSim code. When evaluating all realizations, conspicuous differences appear in addition to the obvious similarities (fig. 11). A mutual, communicating fracture system with a NE-SW strike appears in each model in the SE part of the area. The N-S oriented network in the western end also becomes rather stable. Each model agrees that these two large fracture subsystems do not communicate with each other. Evaluation of the role of the third-largest system in the north is, nevertheless, much less obvious. Some models suggest that it communicates with that in the SE, while other realizations find connection improbable (fig. 11). The reason for the virtual controversy of these models must be that the northern subsystem is close to the percolation threshold. In the case of this class of fracture networks connectivity cannot be predicted; there is a possibility to develop both communicating and non-communicating fracture systems within the given geometrical circumstances. An identical situation appears in the SW part of the area, where the role of numerous small subsystems becomes obscure. There is no way to decide whether they are linked with the neighbouring systems or not. It is essential that, in harmony with the suggestions of the parameter maps, a hardly fractured block appears in the middle of the studied underground site. It is also suggested that the fracture system in this middle zone represents a network well below the percolation threshold, that is, the fracture network remains unconnected even if *D* value is significantly underestimated, while *E* is overestimated. This image is very well in agreement with the general structural concept of the presence of a “less transmissive block” surrounded by NE-SW- and NW-SE-oriented, more transmissive zones, characteristic of the Mórágy Granite body. This connectivity pattern does not change at all if each fracture shorter than 1, 2 or even 5 m is deleted in the model. Deletion of the shortest and thinnest fractures mimics their closure and so simulates the role of vein cementation. Such pattern stability argues for the results of Benedek et al. (2009) and suggests that the compartmentalized appearance of the fracture system is rather the result of geometry *versus* vein cementation.

Fractured porosity maps have been computed for nets with grid cells of 10, 20, 30, 40, 50 and 60 m in side length. To do so, the aperture was given using $a/L = 3*10^{-2}$ determined by detailed analysis of the hand specimen. This ratio is within the typical range given by numerous authors for Mode II fractures (a/L~$3*10^{-3}$–$3*10^{-2}$) in numerous previous studies (Opheim and Gudmundsson, 1989, Vermilye and Scholz, 1995). Average porosity values are presented in Table 2. With increasing cell size, the variation coefficient of the calculated porosities decreases monotonously, proving that porosity values calculated for small cells should not be accepted. The representative elementary volume (REV, Bear, 1972) concerning porosity for the studied granite body can be defined by the cell size, where the variation coefficient becomes stable (M. Tóth and Vass, 2011). On this basis, the aforementioned calculations suggest a REV of ~50 m. For this grid net the average porosity is 1.62% with a maximum of ~6%. Porosity values do not change significantly even if each fracture with an aperture < 0.5 cm is closed in the model simulating the role of fracture cementation.

Using the same cell size (50-m), the minimal values in the diagonal of the 3×3 permeability tensor are $2.34*10^{-14}$, $1.89*10^{-14}$ and $1.22*10^{-14}$ m^2. Here, in the most intensely fractured zones, these values are three orders of magnitude greater, being $1.71*10^{-11}$, $1.62*10^{-11}$ and $1.28*10^{-11}$ m^2. These values are in the same order of magnitude as those measured by Balla et al. (2004). Average permeability tensor values are listed in Table 3, while the xy, yz and xz sections of the average ellipsoid are shown in fig. 12. In good agreement with the fracture network geometry, the permeability suggests a pronounced NE-SW anisotropy of the structure. Of course, these permeabilities concern exclusively the fracture system itself and are based on the assumption that fluid moves only along fractures. Provided percolation occurs also along the near-vein zones, permeability values may be slightly greater, while vein cementation may decrease it significantly. This effect nevertheless does not modify the orientation of the permeability field at all.

Conclusions – Fracture network of the Mórágy Granite

Multiscale evaluation of the fracture network of the Mórágy Granite body clearly proved some essential features can be utilized for understanding the hydraulic behaviour of this system. On the *E-D* plot of the whole study area (fig. 4), parameters measured at different scales of the large outcrop occur rather close to each other. This plot, first of all, proves scale-invariant geometry of the fracture system studied concerning both key parameters. Second, the results of variography at the underground site showed that measurable fracture geometry parameters behave as regionalized variables and thus can be extended spatially. While this second feature makes interpolation and extrapolation of the parameters valid even for the unknown parts of the study area, the first feature warrants the possibility of upscaling the pattern when simulating the fracture network. Thus, one can assume that models generated by the fractal geometry based on RepSim code are reliable and mimic the real fracture geometry accurately.

The results of the simulation clearly show that fracture network characteristics vary remarkably with lithology. While in the monzonite-dominated realm a sparse network of long fractures is typical, in the more felsic monzogranite covariation of E and D is characteristic.

Modelling also shed light on the main directions of the anisotropic fracture system of the granitoid body. The well-defined NE-SW orientation of the system is proved both at the scale of the whole study area and at the underground site. These zones coincide fairly well with the most essential structural lines of the area, proving that seismic lines should be surrounded by intensely deformed aureoles. It is worth emphasizing that in these models, zones of high fracture density at the map scale were delineated exclusively using microfracture data. Good agreement between the mapped major faults and simulated communicating fracture zones is also evident at the repository site. Moreover, the spatial position of the communicating fracture subsystems suggested by the model fits very well with the results of the local hydraulic measurements. On the other hand, the excellent fit between the patterns defined by the main structural zones and the simulated fracture network proves that even large fracture zones can be mapped by a proper fracture system modelling process and a microfracture dataset. Modelling nevertheless must be based on geometric data precisely measured on the real fractured rock body.

Acknowledgements

This project has received funding from the European Union’s Horizon 2020 research and innovation programme under grant agreement No. 654100. Thanks to L. Kovács for the JointMetriX3D data. Cooperation in evaluating digitized fracture network images is acknowledged for R. Kamera. Thorough reviews of Roberto Rizzo and Gyula Dankó are thanked.

References

Anders, M. A., Laubach, S. E., Scholz, C., H. (2014) Microfractures: A review. Journal of Structural Geology 69, 377–394.

Balla, Z. (ed.) (2004): Annual report of the Geological Institute of Hungary, 2003.

Balla Z., Horváth I., Tóth Gy., Benedek K., Mező Gy., Molnár P. (2004): Hydrogeological pattern of the Bátaapáti (Üveghuta) site. Ann. Report Geol. Inst. Hung., 449–472.

Barton, C. C., Larsen, E. (1985): Fractal geometry of two-dimensional fracture networks at Yucca Mountain, Southwestern Nevada. In: Stephanson, O. (ed.): Proc. Int. Symp. on Fundamentals of Rock Joints, 77–84

Barton, C. C. (1995): Fractal analysis of scaling and spatial clustering of fractures. In: Barton, C. C., La Pointe, P. R. (eds.): Fractals in the Earth Sciences. Plenum Press, New York, pp. 168.

Bauer M., M. Tóth, T. (2016): Characterization and DFN modelling of the fracture network in a Mesozoic karst reservoir: Gomba oilfield, Paleogene Basin, Central Hungary. Journal of Petroleum Geology, 40/3, 319–334.

Bean, C. J. (1996): On the cause of 1/f-power spectral scaling in borehole sonic logs. Geophysical Research Letters, 23, 3119–3122.

Bear, J. (1972): Dynamics of fluids in porous media. Elsevier, Amsterdam. pp. 784.

Benedek, K., Dankó, Gy. (2009): Stochastic hydrogeological modelling of fractured rocks: a generic case study in the Mórágy Granite Formation (South Hungary). Geologica Carpathica, 60, 4, 271–281.

Benedek, K., Molnár, P. (2013): Combining structural and hydrogeological data: Conceptualization of a fracuture system. Engineering Geology 163, 1–10.

Benedek, K., Bőthi, Z., Mező, Gy., Molnár, P. (2009): Compartmented flow at the Bátaapáti site in Hungary. Hydrogeology Journal 17, 1219–1232.

Clark, I. (2010): Statistics or geostatistics? Sampling error or nugget effect? Journal of the Southern African Institute of Mining and Metallurgy 110(6),13–18.

de Dreuzy J. R., Davy, P., Bour, O. (2002): Hydraulic properties of two-dimensional random fracture networks following power law distributions of length and aperture. Water Resources Research, 38/12, 121–129.

Deák, F., Molnos, I. (2007): Application of JointMetriX3D in geotechnical documentation of the Bátaapáti shafts. Török Á., Vásárhelyi B. (eds): Mérnökgeológia-Kőzetmechanika 2007, 11–18. (in Hungarian)

Diezte, S., Schmidt, J. W. (1988): Determination of Shape Preserving Spline Interpolants with Minimal Curvature via Dual Programs. Journal of approximation theory, 52, 43–57.

Gaich, A., Schubert, W., Pötsch, M. (2005): Three-dimensional rock mass documentation in conventional tunnelling using JointMetriX3D. Underground Space Use: Analysis of the Past and Lessons for the Future. Taylor & Francis Group, London, 59–64.

Gudmundsson, A. Berg, S. S., Lyslo, K. B., Skurtveit, E. (2001): Fracture networks and fluid transport in active fault zones. Journal of Structural Geology, 23/2-3, 343–353.

Healy, D., Rizzo, R. E., Cornwell, D. G., Farrell, N. J. C., Watkins, H., Timms, N. E., Gomez-Rivas, E., Smith, M. (2017): FracPaQ: A MATLAB™ toolbox for the quantification of fracture patterns. Journal of Structural Geology, 95, 1–16.

Hirata, T. (1989): Fractal dimension of fault system in Japan: fracture structure in rock fracture geometry at various scales. Pure and Applied Geophysics, 131, 157–170.

Katsev, S., L'Heureux, I. (2003): Are Hurst exponents estimated from short or irregular time series meaningful? Computers and Geosciences, 29/9, 1085–1089.

Király, E. (2010): Magmatic evolution of the Mórágy Granite (SE Transdanubia, Hungary). Annual Report of the Geological Institute of Hungary 2009, pp. 41–45.

Király, E., Koroknai, B. (2004): The magmatic and metamorphic evolution of the north-eastern part of the Mórágy Block. Annual Report of the Geological Institue of Hungary 2003, 299–300.

Koike, K., Ichikawa, Y. (2006): Spatial correlation structures of fracture systems for deriving a scaling law and modeling fracture distributions. Computers and Geosciences, 32/8, 1079–1095.

Korvin, G. (1992): Fractal Models in the Earth Sciences. Elsevier, pp. 396.

Kranz, R. L. (1994): Fractal point patterns and fractal fracture traces. In: Nelson, Laubach, (eds.): Rock mechanics. Balkema, Rotterdam, 793–800.

La Pointe, P. R. (1988): A method to characterize fracture density and connectivity through fractal geometry. International Journal of Rock Mechanics and Mining Sciences, Geomech. Abstr., 25, 421–429.

Long, J. C. S. (ed.) (1996): Rock fractures and fluid flow: contemporary understanding and applications. National Academy Press, Washington D. C., pp. 551

M. Tóth, T. (2010): Determination of geometric parameters of fracture networks using 1D data. Journal of Structural Geology, 32, 878–885.

M. Tóth, T., Vass, I. (2011): Relationship between the geometric parameters of rock fractures, the size of percolation clusters and REV. Mathematical Geosciences, 43, 75–97.

Mandelbrot, B. B. (1983): The Fractal Geometry of Nature. Freeman, New York, pp. 468.

Mandelbrot, B. B. (1985): Self-affine fractal dimension. Physica Scripta, 32, 257–260.

Maros, Gy., Palotás, K. (2000): Evaluation of planar features in boreholes Üh–22 and Üh–23 near Üveghuta with CoreDump software. Annual Report of the Geological Institue of Hungary 1999, 315–339.

Maros, Gy., Koroknai, B., Palotás, K., Fodor, L., Dudko, A., Forián-Szabó, M., Zilahi-Sebess, L., Bán-Győry, E. (2004): Tectonic analysis and structural evolution of the north-eastern Mórágy Block. Annual Report of the Geological Institue of Hungary 2003, 370–386.

Maros, Gy., Koroknai, B., Palotás, K., Musitz, B., Füri, J., Borsody, J., Kovács-Pálfy, P., Kónya, P., Viczián, I.,Balogh, K., Pécskay, Z. (2010): Brittle fault zones in the Mórágy Granite (South Transdanubia): new structural and K-Ar data. Annual Report of the Geological Institue of Hungary 2009, pp. 91–112.

Marsan, D., Bean, C. J. (1999): Multiscaling nature of of sonic velocities and lithology in the upper crystalline crust. Geophysical Research Letters, 26, 275–278.

Matheron, G. (1963): Principles of geostatistics. Economic Geology. 58 (8), 1246–1266.

Matsumoto, N., Yomogida, K., Honda, S. (1992): Fractal analysis of fault systems in Japan and the Philippines. Geophysical Research Letters, 19/4, 357–360.

Min, K. B., Jing, L., Stephansson, O. (2004): Determining the equivalent permeability tensor for fractured rock masses using a stochastic REV approach: Method and application to the field data from Sellafield, UK. Hydrogeology Journal, 12/5, 497–510.

Molnár, P., Szebényi, G., Kovács, L. (2010): Preliminary geological interpretation of the Bátaapáti Site. Manuscript, PURAM, Paks, RHK-K-108/10. (in Hungarian)

Neuman, S. (2005): Trends, propects and challenges in quantifying flow transport through fractured rocks. Hydrogeology Journal 13, pp. 124–147.

Neuzil, C. E., Tracy, J. V. (1981): Flow through fractures. Water Resourches Research, 17/1, 191–199.

Oda, M. (1985): Permeability tensor for discontinuous rock masses. Geotechnique, 35, 483–495.

Odling, N. E. (1993): An investigation into the permeability of a 2D natural fracture pattern. Memoirs XXIVth Congress International Association Hydrogeologists, Oslo, pp. 291–300.

Opheim, J. A., Gudmundsson, A. (1989): Formation and geometry of fractures, and related volcanism, of the Krafla fissure swarm, northeast Iceland. Bulletin of the Geological Society of America, 101, 1608–1622.

Ortega, O. J., Marrett, R. A., Laubach, S. E. (2006): A scale-independent approach to fracture intensity and average spacing measurement. AAPG Bulletin, 90/2, 193–208.

Pannatier, Y. (1996): VARIOWIN: Software for spatial data analysis in 2D. Springer, Berlin, Heidelberg and New York

Pollard, D. D., Segall, P. (1987): Theoretical displacements and stresses near fractures in rock: with application to faults, joints, veins, dikes and solution surfaces. In: Atkinson, B. (ed.): Fracture Mechanics of Rock. Academic Press, London

Rizzo, R. E., Healy, D., De Siena, L. (2017): Benefits of maximum likelihood estimators for fracture attribute analysis: Implications for permeability and up-scaling. Journal of Structural Geology 95, 17–31.

Roberts, S., Sanderson, D. J., Gumiel, P. (1998): Fractal analysis of the Sn-W mineralization from central Iberia: Insights into the role of fracture connectivity in the formation of an ore deposit. Economic Geology, 93, 360–365.

Rotár-Szalkai, Á., Eper-Pápai, I., Mentes, Gy. (2006): Well level data analysis in Hungary near a fault region. Journal of Geodynamics 41, 183–189.

Szongoth, G., Zilahi-Sebess, L., Szücsi, P. (2004): Well logging at the Bátaapáti (Üveghuta) site. Annual Report of the Geological Institute of Hungary 2003, 119–134.

Trusoft International Inc (1997): Benoit 1.0 (Trusoft, St. Petersburg, Florida).

Tsuchiya, N., Nakatsuka, K. (1995): A two-dimensional mono-fractal approach to natural fracture networks in rock. Geotherm. Sci. Tech., 6, 63–82.

Turcotte, D. L. (1992): Fractals and chaos in geology and geophysics. Cambridge University Press, pp. 221.

Vermilye, J. M., Scholz, C. H. (1995): Relation between vein length and aperture. Journal of Structural Geology, 17/3, 423–434.

Weiss, J. (2001): Fracture and fragmentation of ice: a fractal analysis of scale invariance. Engineering Fracture Mechanics, 68/17-18, 1975–2012.

Witherspoon, P. A., Wang, J. S. Y., Iwai, K., Gale, J. E. (1980): Validity of cubic law for fluid flow in deformable rock fracture. Water Resources Research, 16/6, 1016–1024.

Yielding, G., Walsh, J. J., Watterson, J. (1992): The prediction of small scale faulting in reservoirs. First Break, 10, 449–460.

Zilahi-Sebess L., Mészáros F., Szongoth G. (2003): Characterisation of fracture zones in granite, based on well-logging data at the Üveghuta site. Annual Report of the Geological Institute of Hungary 2002, 253–266.

Zimmerman, R. W., Bodvarsson, S. (1996): Hydraulic conductivity of rock fractures. Transport in Porous Media, 23/1, 1–30.

Figures, tables

Fig. 1 Location of the study area in Hungary. Inset: Geological sketch map of the study area. Rectangle denotes position of fig. 2, black dot shows the locality of the studied wall.

Fig. 2 Simplified geological map of the study area (after Balla, 2004). Pink: monzogranite-dominated realm, green: monzonite-dominated realm. Bold lines denote proven major shear zones. Red dots show wells. Inset: sketch map of the underground site.

Fig. 3 The subvertical wall and the derived fracture network geometric data. A) Digitized fracture network of the granite wall. The 12 segments of the wall evaluated independently are shown. B) Length distribution of the representative fracture trace segment of the wall. C) log-log transformed distribution function of length data. Arrows denote misfit at the two ends. D) Fracture network of the representative segment of the wall. E) Result of the box-plot calculation.

Fig. 4 *D* and *E* values measured at different scales in the Mórágy granite body.

Fig. 5 *D*-log along the studied wells (well numbers are given at the upper side of the graph). Dimension values in each box vary between 1 and 2.

Fig. 6 Near-well fracture model of a representative well (Üh-22). A) Vertical variation of the *D* parameter. B) Total fracture network model of the well. C) Connected subsystems along the well. D) Hydraulic head profile (after Benedek and Dankó, 2009).

Fig. 7 Pseudo-3D fracture network model for the whole study area. A) Midpoints of the connected fracture subsystem projected to the surface. B) Horizontal fracture network at 0 m a.s.l.; red dots denote wells. C) Vertical AA' section of the fracture network model. Red lines denote known fault zones (after Balla, 2004), and the green line shows the border between monzonite- and monzogranite-dominated areas.

Fig. 8 Semivariograms of the main geometric parameters based on underground data. A) Omnidirectional semivariogram of *E*. b) Omnidirectional semivariogram of *D*. c) SW-NE directional semivariogram of *D*. d) NW-SE directional semivariogram of *D*. In each plot *h* indicates distance between points (Matheron, 1963)

Fig. 9 Variogram surfaces calculated for the underground site for a) *D* and b) *E*. For details see text.

Fig. 10 Spatial distribution of the fracture network parameters at the underground site. a) Map of *D*. b) Discretized map of *D* used for RepSim simulation. c) Map of *E*. d) Discretized map of *E* used for RepSim simulation. Red dots show sampling points.

Fig. 11 Alternative fracture network models simulated for the underground site. Figures show results of different runs. Colours denote interconnected subsystems. a) Total fracture network of a selected run. b) Communicating subsystems of the same run. c-f) Communicating subsystems resulting from different runs. f) Fracture groups denoted by Roman numerals show the most stable topology based on 10 independent runs.

Fig. 12 Sections of the average intrinsic permeability tensor calculated for the underground site (all data in m^2). a) xy section; anisotropy: 1.35, max: 40°. b) yz section; anisotropy: 1.28, max: 167°. c) xz section; anisotropy 1.40, max: 164°.

Table 1 Abbreviations used in fracture network modelling

Abbreviation	Meaning
L	length of a fracture in 3D
l	trace length of a fracture in 2D
a	aperture of a fracture
α	dip direction of a fracture
β	dip angle of a fracture
N	number of fractures
D	fractal dimension in general
E, F	parameters of the length distribution function ($N(L) = F * L^{-E}$)
A, B	parameters of the aperture function ($a = A * L + B$)
Φ	fractured porosity

Table 2 Calculated fractured porosity values for the underground repository site

Cell size (m)	Φmin (%)	Φmax (%)	Φaverage (%)	Standard deviation	Variation coefficient
10	0.00	29.57	2.15	2.84	1.32
20	0.05	17.25	2.22	2.24	1.01
30	0.01	11.57	1.91	1.72	0.90
40	0.25	7.76	1.81	1.50	0.83
50	0.29	5.71	1.70	1.20	0.71
60	0.18	5.17	1.35	1.17	0.87

Table 3 Values of the average permeability tensor calculated for the repository site

3.20E-12	4.56E-13	-2.49E-13
4.56E-13	3.01E-12	-1.52E-13
-2.49E-13	-1.52E-13	2.41E-12

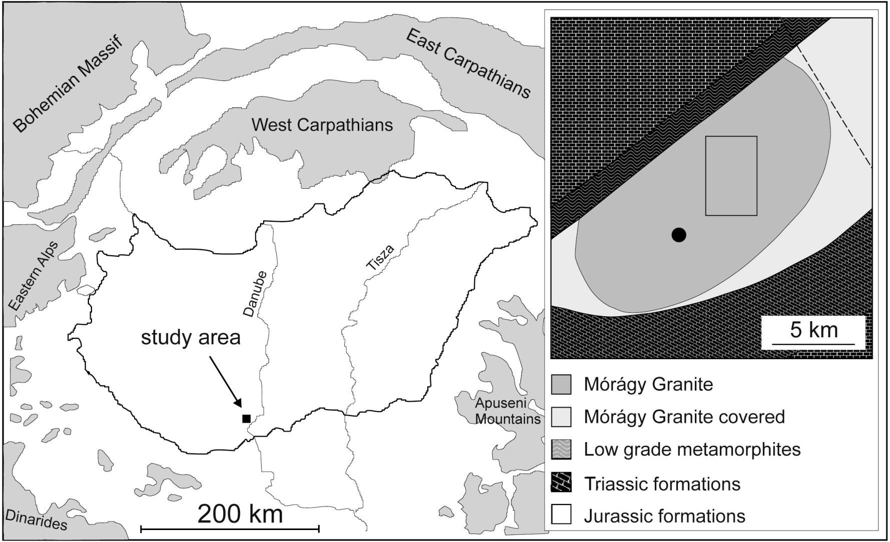
Bohemian Massif
East Carpathians
West Carpathians
Eastern Alps
Danube
Tisza
study area
Apuseni Mountains
Dinarides
200 km
5 km
Mórágy Granite
Mórágy Granite covered
Low grade metamorphites
Triassic formations
Jurassic formations

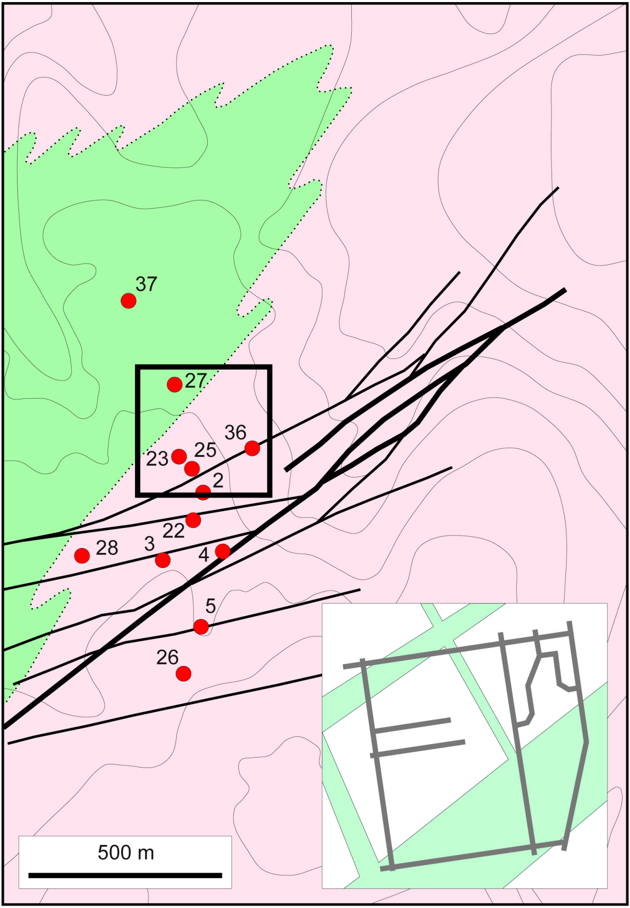
37
27
36
23
25
2
22
28
3
4
5
26
500 m

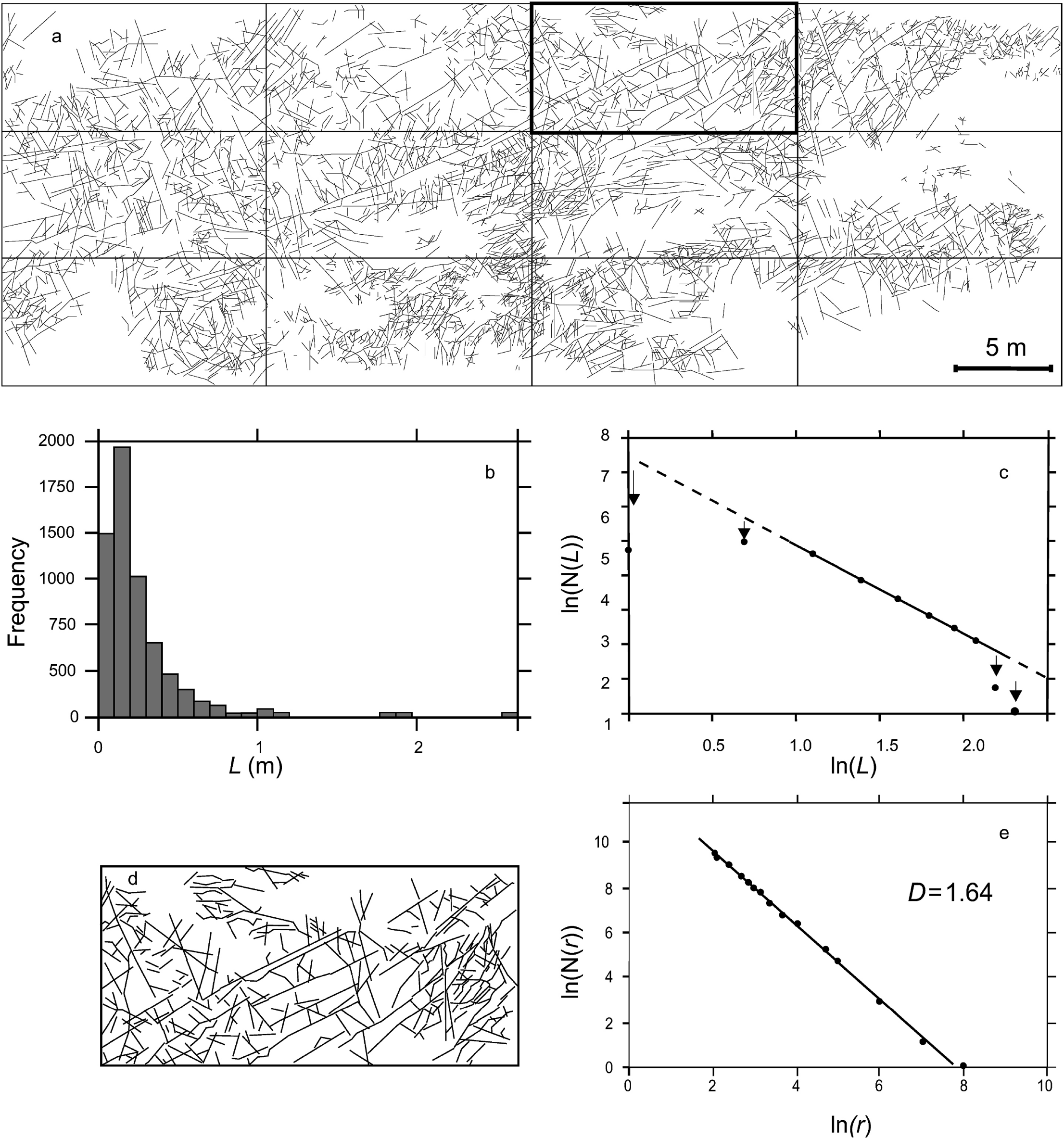

a
5 m
b
Frequency
2000
1750
1500
1250
1000
750
500
250
0
0
1
2
L (m)
c
ln(N(L))
8
7
6
5
4
3
2
1
0.5
1.0
1.5
2.0
ln(L)
d
e
ln(N(r))
10
8
6
4
2
0
0
2
4
6
8
10
D = 1.64
ln(r)

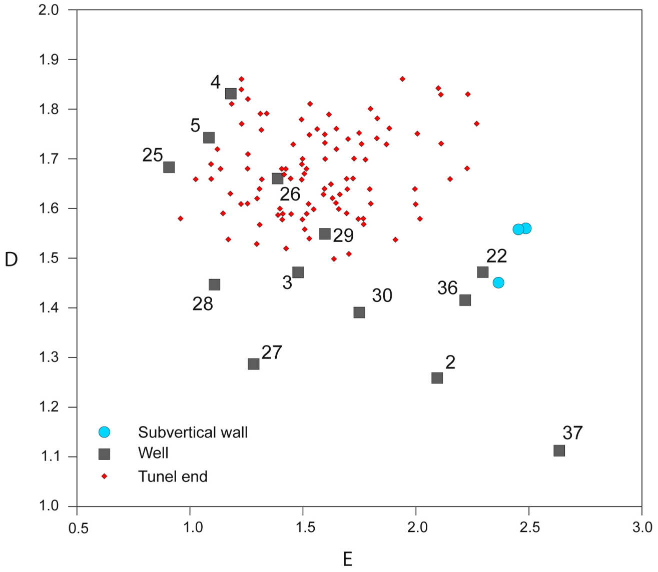
2.0
1.9
1.8
1.7
1.6
1.5
1.4
1.3
1.2
1.1
1.0
D
0.5
1.0
1.5
2.0
2.5
3.0
E
4
5
25
26
29
3
28
27
30
22
36
2
37
Subvertical wall
Well
Tunel end

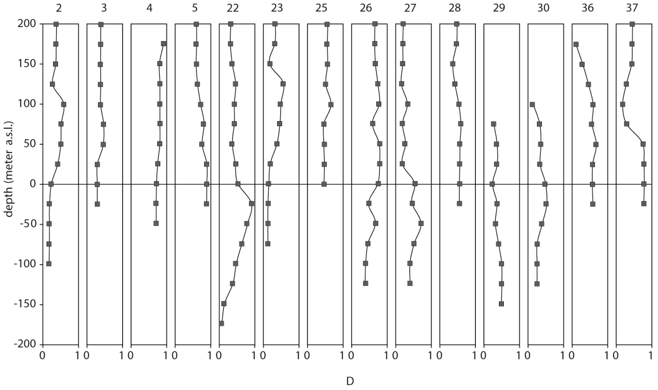

2
3
4
5
22
23
25
26
27
28
29
30
36
37
depth (meter a.s.l.)
200
150
100
50
0
-50
-100
-150
-200
0
1
D

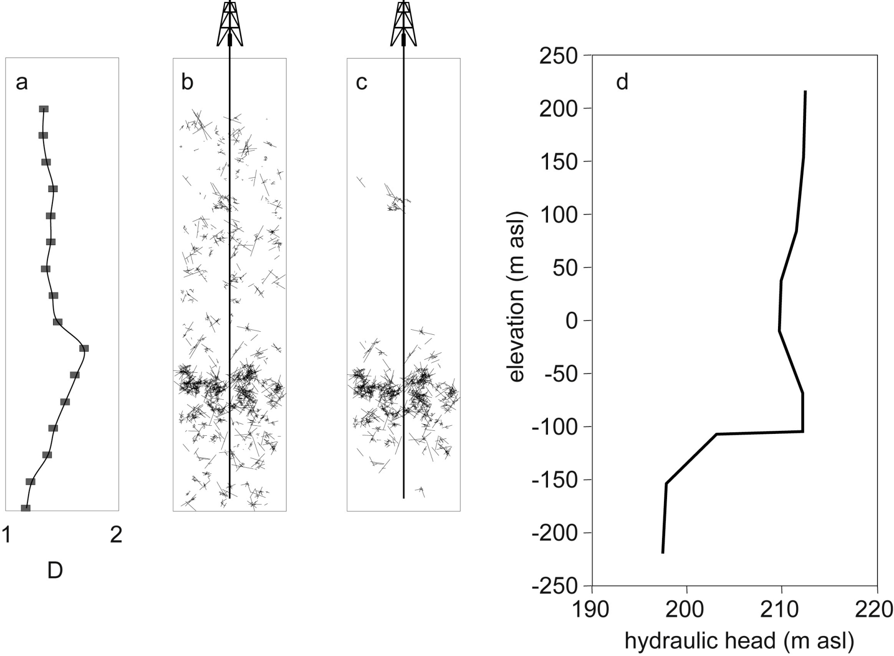
a
b
c
d
1
2
D
elevation (m asl)
hydraulic head (m asl)
250
200
150
100
50
0
-50
-100
-150
-200
-250
190
200
210
220

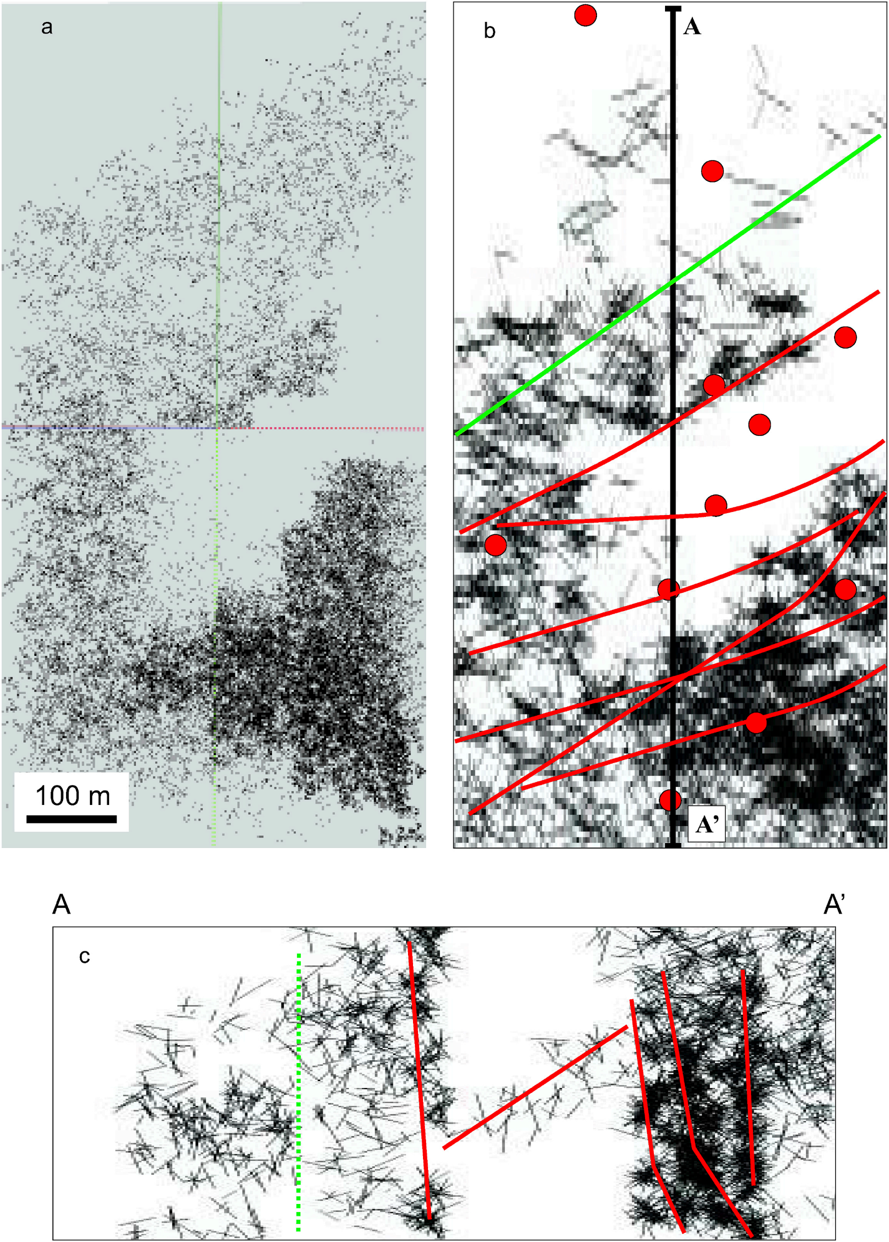

a
100 m
b
A
A'
A
A'
c

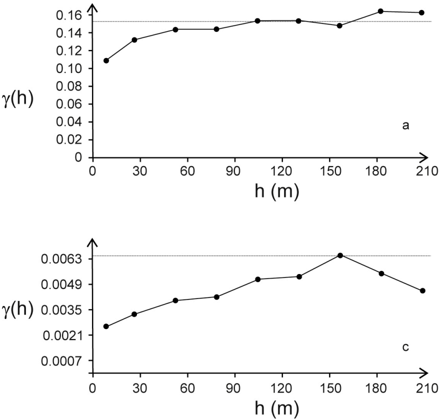

γ(h)
0.16
0.14
0.12
0.10
0.08
0.06
0.04
0.02
0
a
0
30
60
90
120
150
180
210
h (m)
γ(h)
0.0072
0.0056
0.0040
0.0024
0.0008
b
0
30
60
90
120
150
180
210
h (m)
γ(h)
0.0063
0.0049
0.0035
0.0021
0.0007
c
0
30
60
90
120
150
180
210
h (m)
γ(h)
0.010
0.008
0.006
0.004
0.002
d
0
30
60
90
120
150
180
210
h (m)

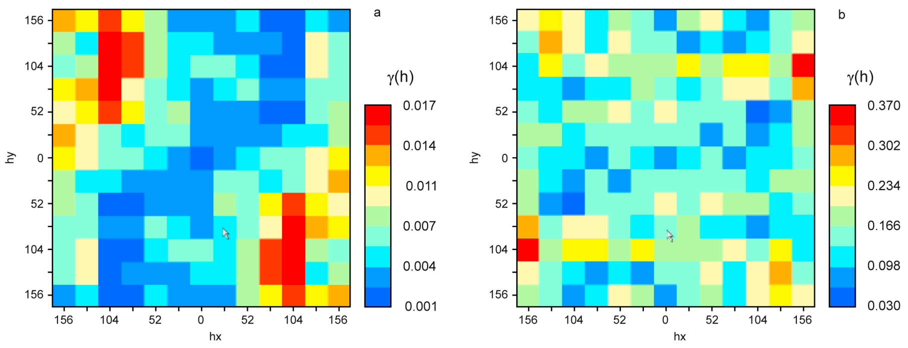
a
b
hy
hx
156
104
52
0
52
104
156
γ(h)
0.017
0.014
0.011
0.007
0.004
0.001
0.370
0.302
0.234
0.166
0.098
0.030

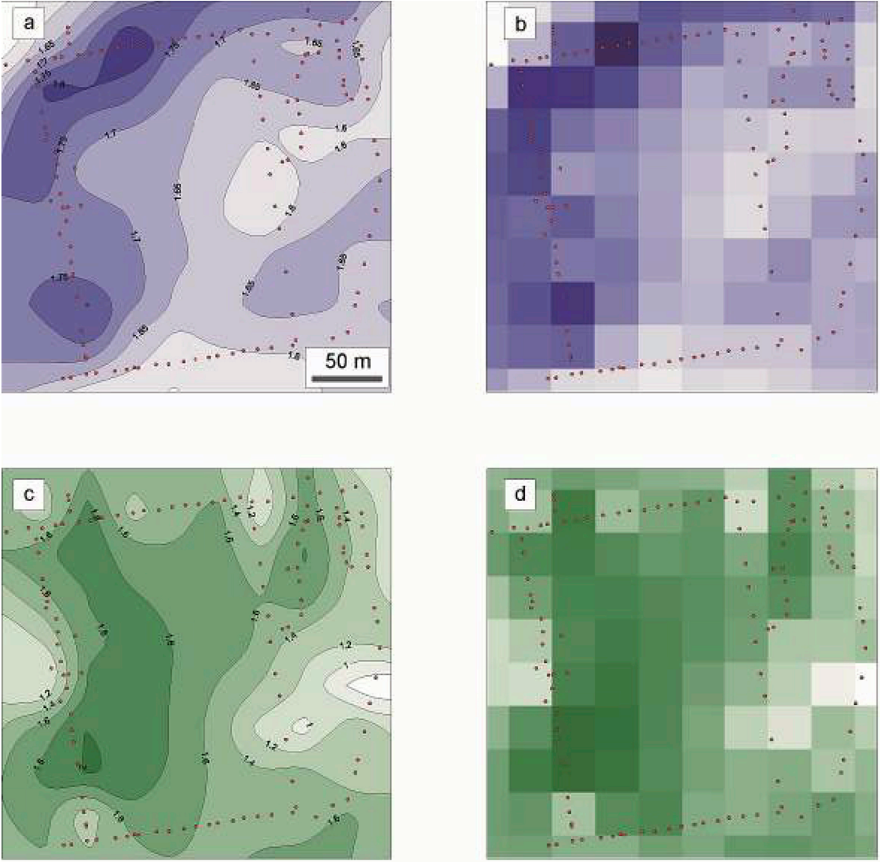

a
b
50 m
c
d

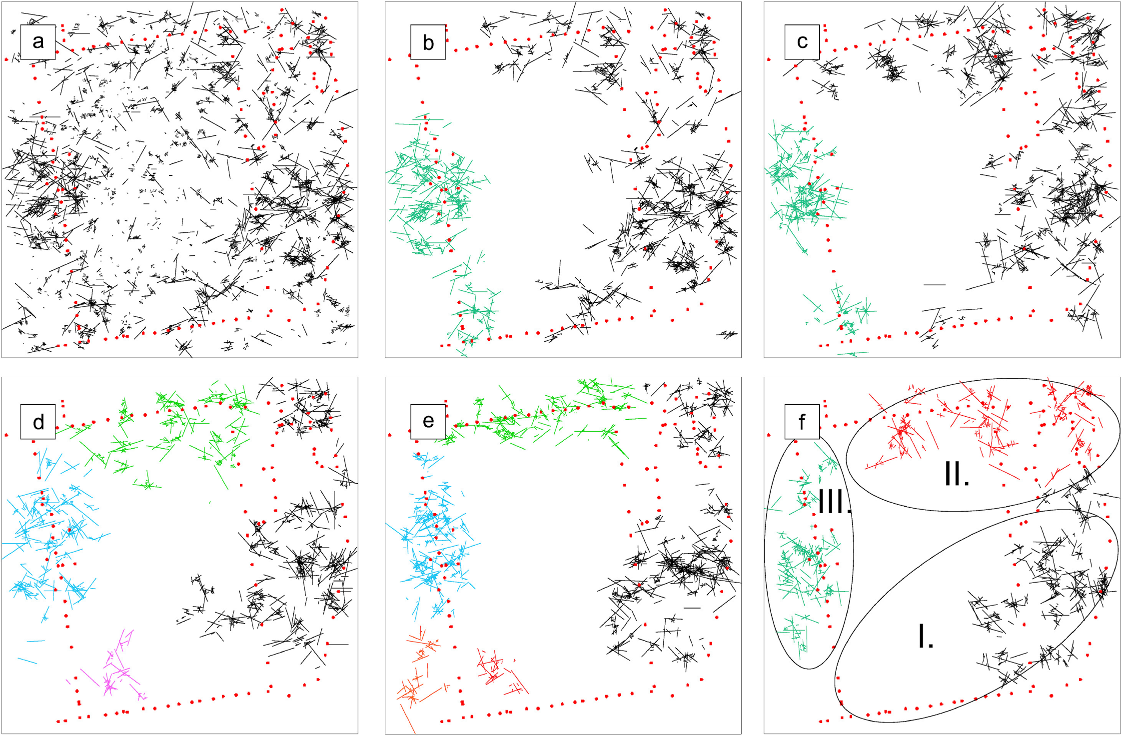
a
b
c
d
e
f
II.
III.
I.

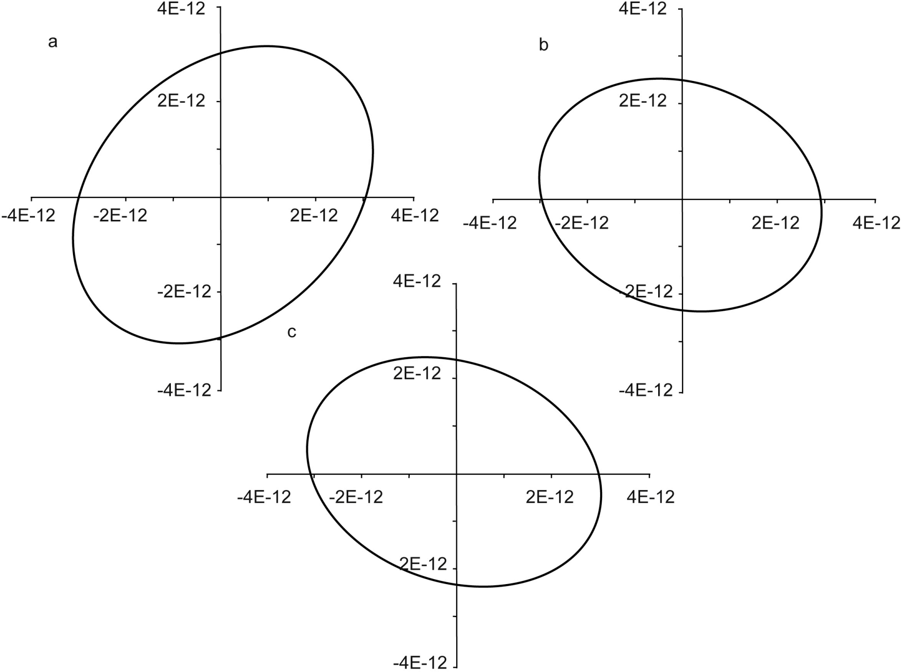
a
b
c
4E-12
2E-12
-2E-12
-4E-12
-4E-12
-2E-12
2E-12
4E-12

Highlights

- Complex study of the fracture system of a fractured granitoid body
- Fracture network characterization in outcrop, wells and underground tunnel ends
- Fractal geometry based DFN model at map scale and in a radioactive waste depository
- Evaluation of hydrodynamic consequences of the fracture network models